Improved Instrument Misalignment Equations for Image Navigation and Registration (INR)

Ahmed Aly Kamel

Abstract Improved misalignment equations are presented for instruments with single scanning mirror and instruments with two scanning mirrors. The improved misalignment equations are derived using Snell's law and Householder transformation. The nominal optical path without misalignments shows that focal plane module reflected image by single mirror rotates by the north-south angle while it does not rotate for two mirrors. The optical path with misalignment of focal plane module to scanner mirror and misalignments within scanner assembly show that the state vector can be represented by six angles for single mirror instruments and by four angles for two mirror instruments. The state vector most significant improvement represents the effect of scan mirror axes orthogonality misalignment angle due to thermal variation and measurement errors. This improvement is shown to be in the north-south direction and equals to the orthogonality misalignment angle multiplied by the tangent of the east-west scan angle.

1 Introduction

The purpose of this paper is to improve instrument misalignment equations and the corresponding h_m matrix in Eq. (18) and sections 3.6 and 5 of Ref. [1]. For single mirror instruments, section 2 describes the optical path without misalignments and section 3 describes the optical path with misalignments of Focal Plane Module (FPM) to scanner mirror and misalignments within scanner assembly. Section 4 derives the improved h_m matrix to replace the h_m matrix in Refs. [1,2] as well as Eqs. (5) and (6) in Ref. [3]. Section 5 shows the effect of the improved misalignment equations due to the scan axes orthogonality angle O_m can be up to 0.2 O_m on image navigation and up to 0.3 O_m on within frame registration for instruments like those used in GOES I-M [4] and MTSAT-1R [5]. Section 5 also compares the improved misalignment equations to the Parametric Systematic Error Correction (ParSEC) equations of Refs. [6,7]. Sections 6 and 7 derive the misalignment equations for two mirror instruments and compare it to the improved single mirror misalignment equations.

Ahmed Aly Kamel
Kamel Engineering Services, Los Angeles, USA, ahmed@kamelengineering.com

1.1 Reference Frames Definitions

The following reference frames from Ref. [1] are relevant to the discussion in this paper.

LOS Reference Frame (LRF)

This frame represents nominal Line of Sight (LOS) vector components. It is attached to the ideal instrument nadir position with no misalignments. The scan angles (E_{LRF}, N_{LRF}) are positive East and North, where N_{LRF} is a rotation about X_{LRF} axis and E_{LRF} is a rotation about the rotated Y-axis.

Instrument Internal Reference Frame (IIRF)

This frame is misaligned relative to LRF. It is attached near the instrument mounting frame to spacecraft. The (E_{IIRF}, N_{IIRF}) are positive East and North, where N_{IIRF} is a rotation about X_{IIRF} axis and E_{IIRF} is a rotation about the rotated Y-axis. Misalignments produced by thermoelastic deformation and biases prevent IIRF axes to be ideally parallel to LRF axes.

Attitude Control Frame (ACF)

This frame represents spacecraft control system. It is attached to spacecraft center of gravity. Misalignments produced by thermoelastic deformation and biases prevent ACF axes to be ideally parallel to the IIRF axes. ACF is rotated relative to IIRF by the (roll, pitch, yaw) attitude correction angles (ϕ_{corr}, θ_{corr}, ψ_{corr}).

2 Single Mirror Optical Path without Misalignments

Although photons travel from Earth and Stars to the FPM detectors, analysis of pointing errors is simpler if the ray path is assumed to originate at the detector. The simplified Fig. 1

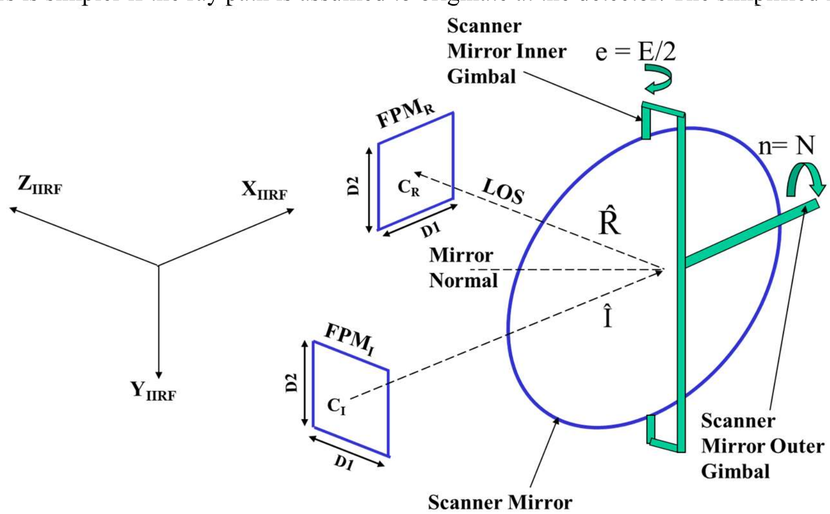

Fig. 1 Relation of Reflected Optical Path to Incident Optical Path

uses this approach to show the relation of the reflected optical path (represented by unit vector $\widehat{R}$) to the incident optical path (represented by the unit vector $\hat{I}$) that emanates from the center C_I of FPM image (FPM_I) at the telescope port near the scanner mirror. The (X_{IIRF}, Y_{IIRF}, Z_{IIRF}) axes shown in Fig. 1 coordinate system axes are defined in Sect. 1.1 and $\widehat{R}$ can be geometrically visualized using Fig. 2. Note that (X_{IIRF}, Y_{IIRF}, Z_{IIRF}) axes are the same as (X_{LRF}, Y_{LRF}, Z_{LRF}) axes when misalignments = 0. Note also that for inverted instruments (i.e., rotated by 180° around Z-axis), (E, N) are positive (West, South) instead of (East, North) and, therefore, (E, N) should be replaced by −(E, N) in the final equations for (E, N) to represent (East, North) angles.

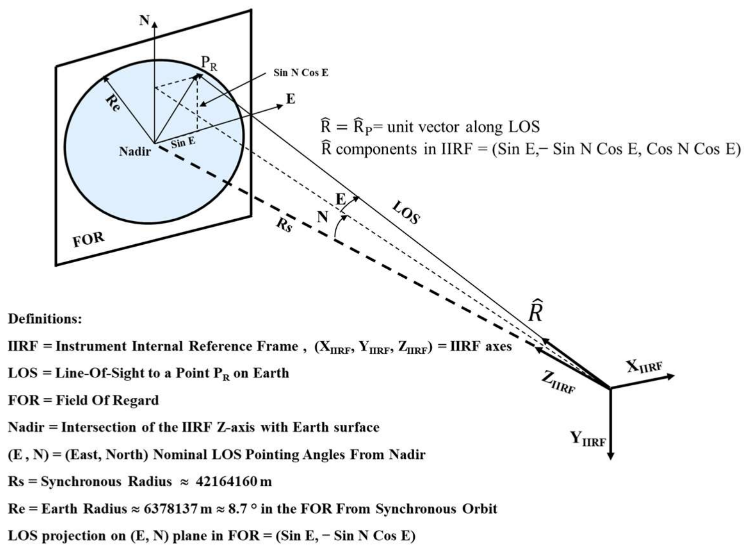

Fig. 2 Geometric Visualization of LOS Projection on FOR

2.1 Instrument Gimbal Angles

In Figs. 1 and 3, (e, n) are rotations about (Y_{IIRF}, X_{IIRF}) axes. The incident unit vector $\hat{I}$ is nominally along the X_{IIRF} axis and the FPM_I is nominally in the (Y_{IIRF}, Z_{IIRF}) plane. In this case, when the scanner mirror is at its home (or nadir) position (i.e., e = n = 0), the reflected unit vector $\widehat{R}$ is along the Z_{IIRF} and the reflected FPM_R is in the (X_{IIRF}, Y_{IIRF}) Plane. Fig. 3 shows that the relation of the optical angle E to the mechanical inner gimbal angle e is E = 2 e based on Snell's law. Note that the relation of the optical angle N to the mechanical outer gimbal angle n is N = n. This is because the outer gimbal axis is parallel to the X_{IIRF} axis. Therefore, the mirror normal would rotate such that a rotation n about the outer gimbal axis would only shift LOS by an angle N = n in the north-south direction. To compute the ray vector from the FPM_I to FPM_R in Fig. 1, the normal to the scan mirror surface must be known.

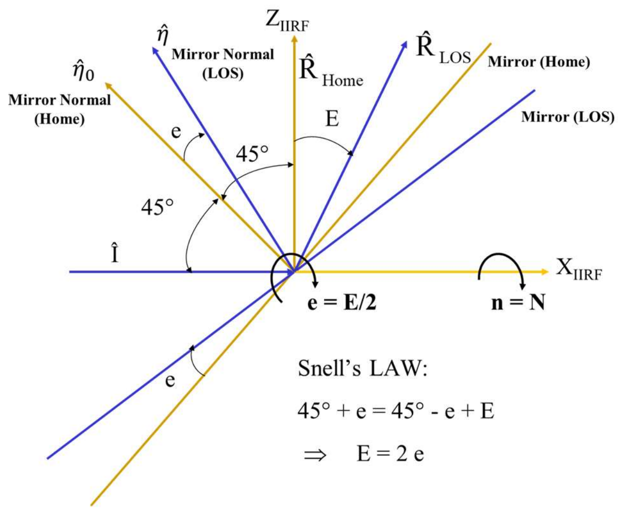

Fig. 3 Relation of Optical Angles (E, N) to Mechanical Angles (e, n)

Figure 3 shows that in the scan home (nadir) position, the mirror normal $\hat{\eta}_0$ has equal Z_{IIRF} and $-X_{IIRF}$ components and a zero Y_{IIRF} component in the IIRF coordinate systems. This leads to:

$$\hat{\eta}_0 = \frac{1}{\sqrt{2}}[-1 \quad 0 \quad 1]^T \tag{1}$$

The unit normal $\hat{\eta}$ is obtained using the following equation (see Ref. [8], Sect. 12.1):

$$\hat{\eta} = \begin{bmatrix} 1 & 0 & 0 \\ 0 & C_n & -S_n \\ 0 & S_n & C_n \end{bmatrix} \hat{\eta}_e \tag{2}$$

Where C_x = Cos x, S_x = Sin x, T_x= Tan x are used throughout this paper.
$\hat{\eta}_e$ is the mirror normal after the scanner inner gimbal angle rotated by angle e and can be obtained from Eq. (A.4) and Fig. A with $(\vec{A}, \vec{B})$ replaced by $(\hat{\eta}_0, \hat{\eta}_e)$:

$$\hat{\eta}_e = \hat{\eta}_0 C_e + \widehat{G}_e(\widehat{G}_e \bullet \hat{\eta}_0)(1 - C_e) + (\widehat{G}_e \otimes \hat{\eta}_0)\, S_e \tag{3.1}$$

When the mirror is at the nominal nadir position, the inner gimbal axis of rotation $\widehat{G}_e$ is along the Y_{IIRF} axis and the mirror normal $\hat{\eta}_0$ is given by Eq. (1). This leads to:

$$\widehat{G}_e = [0 \quad 1 \quad 0]^T,\ \widehat{G}_e \bullet \hat{\eta}_0 = 0,\ \widehat{G}_e \otimes \hat{\eta}_0 = \frac{1}{\sqrt{2}}[1 \quad 0 \quad 1]^T \tag{3.2}$$

Substituting Eqs. (1) and (3.2) in Eq. (3.1) and the resulting equation in Eq. (2), we get:

$$\hat{\eta}_e = \frac{1}{\sqrt{2}}[-X_e \quad 0 \quad Y_e]^T,\ \hat{\eta} = \frac{1}{\sqrt{2}}[-X_e \ \vdots\ -S_n Y_e \ \vdots\ C_n Y_e]^T \tag{4.1}$$

Where

$$X_e = C_e - S_e = (1 - S_E)^{1/2},\ Y_e = C_e + S_e = (1 + S_E)^{1/2} \tag{4.2}$$

2.2 *Incident and Reflected Beams Relationship*

Figure 4 shows the relationship between mirror normal, incident and reflected beams. Note that according to Snell's Law, the incident and reflected beams are geometrically maintained in a plane perpendicular to the mirror surface such that the incident and reflected beams have equal angles relative to the mirror normal. In this case, the relationship between the reflected beam, incident beam, and mirror normal is given by the Householder transformation:

$$\hat{R} = \hat{I} - 2(\hat{\eta} \bullet \hat{I})\hat{\eta} \tag{5.1}$$

Where $\hat{\eta}$ is given by Eq. (4.1) and $\hat{I}$ is a unit vector along the X_{IIRF} axis. This leads to:

$$\hat{\eta} = \frac{1}{\sqrt{2}}\begin{bmatrix} -X_e \\ -S_n Y_e \\ C_n Y_e \end{bmatrix}, \hat{I} = \begin{bmatrix} 1 \\ 0 \\ 0 \end{bmatrix}, \hat{R} = \begin{bmatrix} 1 - X_e^2 \\ -S_n X_e Y_e \\ C_n X_e Y_e \end{bmatrix} = \begin{bmatrix} S_E \\ -S_N C_E \\ C_N C_E \end{bmatrix} \tag{5.2}$$

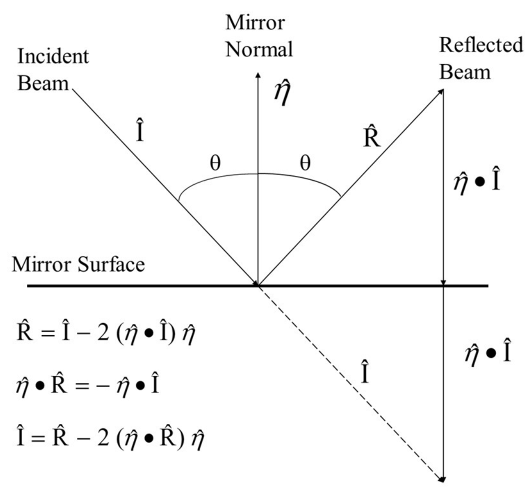

Fig. 4 Relations between Mirror Normal, Incident and Reflected Beams

2.3 *Off-Center Detector Image Reflection*

The off-center detector image reflection can be determined using Eq. (5.1) with the incident unit vector $\hat{I}$ changed to represent a point off the center C_I of the FPM_I image in Fig. 1. Figure 5 shows the case when the point P_I is at $(Y_{IIRF}, Z_{IIRF}) = (b, -a)$ position. In this case, the (Y_{IIRF}, Z_{IIRF}) components of the incident unit vector $\hat{I}$ are $(-b, a)$ and

$$\hat{I} = [c \quad -b \quad a]^T, c = \sqrt{1 - a^2 - b^2} \tag{6}$$

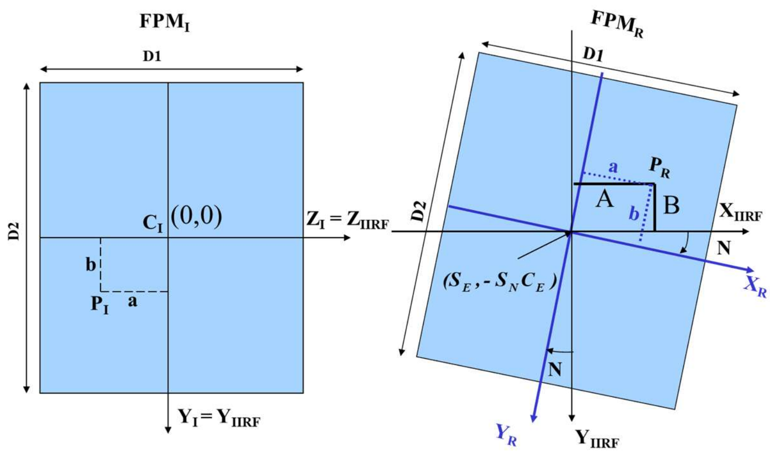

Fig. 5 Mirror Reflection Effect on FPM Image Rotation

Now substituting Eqs. (4.1), (4.2), and (6) in Eq. (5.1), we get $\widehat{R}$ components along (X_{IIRF}, Y_{IIRF}, Z_{IIRF}) axes:

$$\widehat{R} = \begin{bmatrix} \widehat{R}_X \\ \widehat{R}_Y \\ \widehat{R}_Z \end{bmatrix} = c \begin{bmatrix} S_E \\ -S_N C_E \\ C_N C_E \end{bmatrix} + \begin{bmatrix} AC_E \\ AS_N S_E - BC_N \\ -AC_N S_E - BS_N \end{bmatrix} = \begin{bmatrix} S_{E_{LRF}} \\ -S_{N_{LRF}} C_{E_{LRF}} \\ C_{N_{LRF}} C_{E_{LRF}} \end{bmatrix} \tag{7.1}$$

Where,

$$\begin{bmatrix} E_{LRF} \\ N_{LRF} \end{bmatrix} = \begin{bmatrix} \mathrm{Sin}^{-1}(cS_E + AC_E) \\ \mathrm{Tan}^{-1}\left(\frac{cS_N C_E - AS_N S_E + BC_N}{cC_N C_E - AC_N S_E - BS_N}\right) \end{bmatrix} \equiv \begin{bmatrix} E_{IIRF} \\ N_{IIRF} \end{bmatrix} \text{ with no misalignments} \tag{7.2}$$

$$A = a\,C_N + bS_N,\ \ B = bC_N - aS_N \tag{7.3}$$

$$(X_{LRF}, Y_{LRF}, Z_{LRF}) \equiv (X_{IIRF}, Y_{IIRF}, Z_{IIRF}) \tag{7.4}$$

In view of Fig. 5, (A, B) represent the (a, b) components rotated about the FPM_R center (S_E, – S_N C_E) by the NS pointing angle N. Also, the point P_R deviation (ΔR_X, ΔR_Y) from the reflected FPM_R center can be obtained from Eq. (7.1) as follows:

$$\begin{bmatrix} \Delta\widehat{R}_X \\ \Delta\widehat{R}_Y \end{bmatrix} = \begin{bmatrix} S_{E_{LRF}} \\ -S_{N_{LRF}} C_{E_{LRF}} \end{bmatrix} - \begin{bmatrix} S_E \\ -S_N C_E \end{bmatrix} = (c-1)\begin{bmatrix} S_E \\ -S_N C_E \end{bmatrix} + \begin{bmatrix} AC_E \\ AS_N S_E - BC_N \end{bmatrix} \tag{8}$$

where, $(E_{LRF}, N_{LRF}) = (E_{IIRF}, N_{IIRF})$ are the detector (East, North) pointing angles to the point P_R and (E, N) are the Instrument LOS (East, North) scan angles [i.e., = (2e, n), where (e, n) are the corresponding gimbal angles]. Note that (S_E, – S_N C_E) are the components of the reflection of FPM center C_I on the (X_{IIRF}, Y_{IIRF}) plane and is defined as the FPM LOS as shown in Fig. 2.

Now, the deviation in the P_R pointing angles (E_{LRF}, N_{LRF}) from the FPM LOS pointing angle (E, N) can be obtained by substituting $(E_{LRF}, N_{LRF}) = (E, N) + (\Delta E, \Delta N)$ in Eq. (8). Using $C_{x+\Delta x} = C_x - \Delta x\, S_x$, and $S_{x+\Delta x} = S_x + \Delta x\, C_x$ and ignoring the higher order terms in $(\Delta E, \Delta N, a, b)$, we get:

$$\begin{bmatrix} \Delta\hat{R}_X \\ \Delta\hat{R}_Y \end{bmatrix} = \begin{bmatrix} \Delta E\, C_E \\ -\Delta N C_N C_E + \Delta E S_N S_E \end{bmatrix} \cong \begin{bmatrix} A C_E \\ A S_N S_E - B C_N \end{bmatrix} \tag{9.1}$$

$$(\Delta E, \Delta N) \cong (A, B/C_E) \text{ and } (E_{LRF}, N_{LRF}) \cong (E, N) + (A, B/C_E) \tag{9.2}$$

It is important to point out that the nonlinear terms are ignored in Eq. (9.1) because the purpose of this paper is to determine the misalignment effects which is assumed to be < 1000 μrad. In this case, assuming an FPM (D1, D2) = (2°,1°) leads to:

$$|a| \leq D1/2 = 1° = 0.0175 \text{ rad} \Rightarrow a^2 = 0.00031 \text{ rad} \tag{10.1}$$

$$|b| \leq D2/2 = 0.5° = 0.0087 \text{ rad} \Rightarrow b^2 = 0.00007 \text{ rad} \tag{10.2}$$

and when the above (a, b) values are multiplied by a misalignment m = 1000 μrad, we get:

$m \times |a| = 17.5\ \mu\text{rad} \Rightarrow m \times a^2 = 0.31\ \mu\text{rad}$, $m \times |b| = 8.7\ \mu\text{rad} \Rightarrow m \times b^2 = 0.07\ \mu\text{rad}$

Therefore, the linear effect is small but significant and the nonlinear contribution are negligible. Note that, in view of Fig. 5 and Eq. (9.2), the mirror reflects a P_I detector south in the FPM to a P_R point north on Earth, rotates the FPM image by the NS pointing angle N and scales its ΔN deviation by a factor of C_E in the Y_{IIRF} direction. Note also that Tapered Elevation Scan (TES) along X_R direction in Fig. 5 was used in MTSAT-1R to avoid coverage gaps due to FPM reflected image rotation (see Figs. 6 and 7 in Ref. [5]).

3 Single Mirror Optical Path with Misalignments

Even though the best possible alignment techniques and procedures are used, slight misalignment would still exist due to manufacturing tolerances and on-orbit thermal variation within the Instrument optical elements shown in Fig. 1. The following two subsections determine the effect of FPM misalignments relative to scanner assembly and orthogonality misalignments within scanner assembly on optical path as follows:

- FPM center and axes misalignment relative to the scanner assembly represented in Sect. 3.1 by small shift (m_{f1}, m_{f2}) and small rotation m_{f3} relative to $(X_{IIRF}, Y_{IIRF}, Z_{IIRF})$.
- Mirror normal orthogonality misalignment relative to the inner gimbal axis represented in Sect. 3.2 by small rotations $(m_{\eta 1}, m_{\eta 2}, m_{\eta 3})$ about $(X_{IIRF}, Y_{IIRF}, Z_{IIRF})$.
- Inner gimbal axis orthogonality misalignment relative to the outer gimbal axis represented in Sect. 3.2 by small rotations (m_{e1}, m_{e2}, m_{e3}) about $(X_{IIRF}, Y_{IIRF}, Z_{IIRF})$.

Note that the outer gimbal axis orthogonality misalignment does not need to be analyzed. This is because an outer gimbal axis orthogonality misalignment effect is equivalent to an inner gimbal axis orthogonality misalignment plus (roll, pitch yaw) attitude correction $(\phi_{corr}, \theta_{corr}, \psi_{corr})$. Note also that because the above three groups of misalignments are small and independent of each other, their effect on pointing can be obtained separately based on the linear systems superposition principle and their cumulative effect is then obtained by adding their separate effects. This is done in Sect. 4.

3.1 FPM Misalignments to Scanner Assembly

Figure 6 shows the effect of FPM_I misalignment relative to its nominal position shown in Fig. 5. Note that the cumulative effect of various optical elements misalignments can be represented by a shift of the FPM_I center C_I by (m_{f1}, m_{f2}) relative to the nominal position and a rotation angle m_{f3} about the X_{IIRF} axis as shown on the left side of Fig. 6. The misalignment effect on the reflected FPM_R can be obtained following similar steps to that used in the derivation of Eqs. (6) to (9) with the components (a, b) adjusted to include the misalignment effects shown in Fig. 6. Keeping only linear terms in (m_{f1}, m_{f2}, m_{f3}) leads to:

$$a' = m_{f1} + a\,C_{mf3} + b\,S_{mf3} \cong m_{f1} + a + b\,m_{f3} \tag{11.1}$$

$$b' = m_{f2} + b\,C_{mf3} - a\,S_{mf3} \cong m_{f2} + b - a\,m_{f3} \tag{11.2}$$

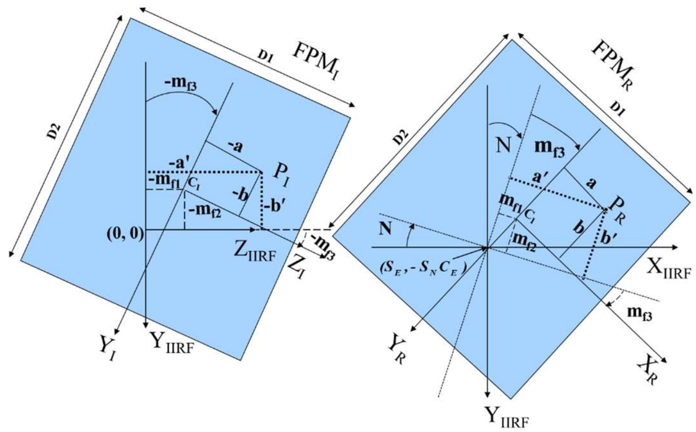

Fig. 6 Instrument Misalignments Effect on the Incident and Reflected FPM

Substituting Eqs. (11.1) and (11.2) in Eq. (7.3), we get:

$$A' = a'\,C_N + b'\,S_N = A + m_{f1}\,C_N + m_{f2}\,S_N + B\,m_{f3} \tag{12.1}$$

$$B' = b'\,C_N - a'\,S_N = B + m_{f2}\,C_N - m_{f1}\,S_N - A\,m_{f3} \tag{12.2}$$

Note that Eqs. (12.1) and (12.2) represent the (X_{IIRF}, Y_{IIRF}) components of the point P_R relative to the FPM LOS. These can be visualized using the right side of Figs. 5 and 6 which are simply a rotation of the figure on the left side by the angle N about a line perpendicular to FPM plane. Substituting Eqs. (12.1) and (12.2) in Eq. (9.2), we get:

$$\Delta E = A' = A - \Delta E_{mf}\,,\quad \Delta N C_E = B' = B - \Delta N_{mf} C_E \tag{13.1}$$

$$\Delta E_{mf} = -m_{f1}\,C_N - m_{f2} S_N - B\,m_{f3},\ \Delta N_{mf}\,C_E = -m_{f2}\,C_N + m_{f1} S_N + A\,m_{f3} \tag{13.2}$$

3.2 *Scanner Assembly Orthogonality Misalignments*

Manufacturing tolerances and thermal distortion within the scanner assembly could lead to a mirror normal that is not orthogonal to the scanner inner gimbal axis (assumed to be orthogonal in Fig. 3). This can be represented by small ($m_{\eta 1}$, $m_{\eta 2}$, $m_{\eta 3}$) rotations of the unit vector $\hat{\eta}_0$ of Eq. (1) about the (X_{IIRF}, Y_{IIRF}, Z_{IIRF}) axes. In this case, the perturbed unit vector $\hat{\eta}_0'$ can be obtained using the transformation $C_{m\eta}$ given by Eqs. (12-22) to (12-24a) in Ref. [8]

$$\hat{\eta}_0' = C_{m\eta}\hat{\eta}_0 \,, \; C_{m\eta} \cong \begin{bmatrix} 1 & m_{\eta 3} & -m_{\eta 2} \\ -m_{\eta 3} & 1 & m_{\eta 1} \\ m_{\eta 2} & -m_{\eta 1} & 1 \end{bmatrix} \tag{14}$$

Note that ($m_{\eta 1}$, $m_{\eta 2}$, $m_{\eta 3}$) expected to be < 1000 μrad, 3-σ, linear approximations $\text{Sin}\alpha = \alpha$ and $\text{Cos}\,\alpha = 1$ used to obtain Eq. (14) would lead to errors < 1.7×10^{-4} μrad for Sinα, and < 0.5 μrad for Cos α which are negligible. Substituting Eq. (1) in Eq. (14), we get:

$$\hat{\eta}_0' = \tfrac{1}{\sqrt{2}}\left[-\left(1 + m_{\eta 2}\right) \vdots\; m_{\eta 1} + m_{\eta 3} \;\vdots\; 1 - m_{\eta 2}\right]^T \tag{15}$$

Similarly, manufacturing tolerances and thermal distortion within the scanner assembly could lead to an inner gimbal axis that is not orthogonal to the outer gimbal axis (assumed to be orthogonal in Fig. 3). This can be represented by small (m_{e1}, m_{e2}, m_{e3}) rotations of the unit vector $\hat{G}_e$ of Eq. (3.2) about the (X_{IIRF}, Y_{IIRF}, Z_{IIRF}) axes. In this case, the perturbed unit vector $\hat{G}_e'$ along the misaligned inner gimbal axis can be obtained from $\hat{G}_e$ using the transformation C_{me} given by Eqs. (12-22) to (12-24a) in Ref. [8]

$$\hat{G}_e' = C_{me}\hat{G}_e = C_{me}\begin{bmatrix} 0 \\ 1 \\ 0 \end{bmatrix}, \; C_{me} \cong \begin{bmatrix} 1 & m_{e3} & -m_{e2} \\ -m_{e3} & 1 & m_{e1} \\ m_{e2} & -m_{e1} & 1 \end{bmatrix}, \; \hat{G}_e' = \begin{bmatrix} m_{e3} \\ 1 \\ -m_{e1} \end{bmatrix} \tag{16}$$

Substituting Eqs. (15) and (16) in Eq. (3.1) and ignoring nonlinear misalignment terms, we get:

$$\hat{\eta}_e = \hat{\eta}_0' C_e + \hat{G}_e'\left(\hat{G}_e' \bullet \hat{\eta}_0'\right)(1 - C_e) + \left(\hat{G}_e' \otimes \hat{\eta}_0'\right) S_e = \tfrac{1}{\sqrt{2}}\begin{bmatrix} -X_e + M_1 \\ M_2 \\ Y_e + M_3 \end{bmatrix} \tag{17}$$

Where X_e and Y_e are given by Eq. (4.2), and

$$M_1 = -m_{\eta 2}Y_e \,, \; M_2 = m_{\eta 1} + m_{\eta 3} - m_{e1} - m_{e3} + m_{e1}Y_e + m_{e3}X_e, \; M_3 = -m_{\eta 2}X_e \tag{18}$$

Substituting Eq. (17) in Eq. (2), we get:

$$\hat{\eta} = \tfrac{1}{\sqrt{2}}\begin{bmatrix} -X_e + M_1 \\ -Y_eS_n + M_2C_n - M_3S_n \\ Y_eC_n + M_2S_n + M_3C_n \end{bmatrix} \tag{19}$$

Substituting Eqs. (6) and (19) in Eq. (5.1) and using Eqs. (7.1) and (7.3), we get:

$$2\left(\hat{\eta} \bullet \hat{I}\right) = \sqrt{2}\left[(-X_e + M_1)c + (Y_e + M_3)A - M_2B\right] \tag{20.1}$$

$$\begin{bmatrix}\hat{R}_X\\ \hat{R}_Y\end{bmatrix} = \begin{bmatrix}S_{E_{LRF}}\\ -S_{N_{LRF}}C_{E_{LRF}}\end{bmatrix} + \begin{bmatrix}\Delta\hat{R}_X\\ \Delta\hat{R}_Y\end{bmatrix} = \begin{bmatrix}S_{E_{IIRF}}\\ -S_{N_{IIRF}}C_{E_{IIRF}}\end{bmatrix} \tag{20.2}$$

$$\begin{bmatrix}\Delta\hat{R}_X\\ \Delta\hat{R}_Y\end{bmatrix} = \begin{bmatrix}2M_1X_e + (M_3X_e - M_1Y_e)A - M_2X_eB\\ X_e(M_2C_n - M_3S_n) + Y_eS_nM_1 - AY_e(M_2C_n - 2M_3S_n) - BY_eM_2S_n\end{bmatrix} \tag{20.3}$$

Using REDUCE algebraic manipulation program [9] for substituting Eqs. (4.2) and (18) in Eq. (20.3), separating the terms containing AS_α and BS_α as modelling errors, and ignoring AS_α^2 and BS_α^2 terms lead to:

$$\Delta\hat{R}_X = -2m_{\eta2}C_E - (m_{\eta1} + m_{\eta3})B + \Delta R_{Xe} \tag{21.1}$$

$$\begin{aligned}\Delta\hat{R}_Y = &-2m_{\eta2}S_NS_E + (m_{\eta1} + m_{\eta3} - m_{e1} - m_{e3})(1 - S_E)^{1/2}C_N\\ &+m_{e1}C_EC_N + m_{e3}(1 - S_E)C_N - (m_{\eta1}+m_{\eta3})A+\Delta R_{Ye}\end{aligned} \tag{21.2}$$

$$\Delta R_{Xe} = 2m_{\eta2}AS_E - m_{Y1}BS_E \tag{21.3}$$

$$\Delta R_{Ye} = -(m_{Y1} + m_{\eta1} + m_{\eta3})AS_E - 2m_{\eta2}AS_N - (m_{\eta1} + m_{\eta3})BS_N \tag{21.4}$$

Where,

$$m_{Y1} = -0.5(m_{\eta1} + m_{\eta3} - m_{e1} + m_{e3}) \tag{21.5}$$

Note that the terms AS_α and BS_α when multiplied by 1000 μrad misalignment are very small and, therefore, are considered as modelling error. If they are found to be significant they can then be added as described in Sect. 4. Note also that $(1-S_E)^{1/2} \approx (1.5 - S_E + 0.5\,C_E)/2$. This leads to:

$$\Delta\hat{R}_Y = -2m_{\eta2}S_NS_E + (m_{Y0} + m_{Y1}\,S_E + m_{Y2}\,C_E)C_N - (m_{\eta1}+m_{\eta3})A+\Delta R_{Ye} \tag{22.1}$$

Where,

$$m_{Y0} = 0.75(m_{\eta1} + m_{\eta3} - m_{e1}) + 0.25\,m_{e3} \tag{22.2}$$

$$m_{Y2} = 0.25(m_{\eta1} + m_{\eta3} + 3m_{e1} - m_{e3}) \tag{22.3}$$

Now, substituting $(E_{IIRF}, N_{IIRF}) = (E_{LRF}, N_{LRF}) - (\Delta E_{mo}, \Delta N_{mo})$ in Eq. (20.2), where, $(\Delta E_{mo}, \Delta N_{mo})$ denote the combined mirror normal and inner gimbal orthogonality misalignments effects on LOS pointing, and ignoring nonlinear terms, we get:

$$\begin{bmatrix}-\Delta E_{mo}\,C_{E_{LRF}}\\ \Delta N_{mo}\,C_{N_{LRF}}C_{E_{LRF}} - \Delta E_{mo}\,S_{N_{LRF}}\,S_{E_{LRF}}\end{bmatrix} = \begin{bmatrix}\Delta\hat{R}_X\\ \Delta\hat{R}_Y\end{bmatrix} \tag{23.1}$$

$$\Delta E_{mo} = -\frac{\Delta\hat{R}_X}{C_{E_{LRF}}} = 2m_{\eta2} + (m_{\eta1}+m_{\eta3})B - \Delta E_{moe} \tag{23.2}$$

$$\begin{aligned}\Delta N_{mo}\,C_E &= \frac{\Delta\hat{R}_Y}{C_{N_{LRF}}}\frac{C_E}{C_{E_{LRF}}} + \Delta E_{mo}T_{N_{LRF}}T_{E_{LRF}}C_E\\ &= (m_{Y0} + m_{Y1}\,S_E + m_{Y2}\,C_E) - (m_{\eta1}+m_{\eta3})A - \Delta N_{moe}\end{aligned} \tag{23.3}$$

Where

$$\Delta E_{moe} = \Delta\hat{R}_{Xe} - 2m_{\eta2}(C_E/C_{E_{LRF}} - 1) \tag{23.4}$$

$$\begin{aligned}\Delta N_{moe} = &-\Delta\hat{R}_{Ye} - (m_{\eta1} + m_{\eta3})(C_NC_E/C_{E_{LRF}}C_{N_{LRF}} - 1)\\ &-2m_{\eta2}(T_{N_{LRF}}T_{E_{LRF}} - S_NS_E)\end{aligned} \tag{23.5}$$

4 Combined Attitude and Misalignment Effect

The combined effect of attitude correction and misalignment can be written as:

$$E_{ACF} = E_{LRF} - \Delta E_{corr} - \Delta E_m,\ N_{ACF} = N_{LRF} - \Delta N_{corr} - \Delta N_m \tag{24}$$

(E_{ACF}, N_{ACF}) = detector pointing angles in ACF defined in Sect. 1.1.
$(\Delta E_{corr}, \Delta N_{corr})$ = detector pointing correction due to the small attitude correction angles $(\phi_{corr}, \theta_{corr}, \psi_{corr})$ defined in Sect. 1.1 and obtained from Eqs. (27) and (29) of Ref. [1]

$$\Delta E_{corr} = \theta_{corr} C_{N_{LRF}} + \psi_{corr} S_{N_{LRF}} \tag{25.1}$$
$$\Delta N_{corr} = \phi_{corr} + \left(\theta_{corr} S_{N_{LRF}} - \psi_{corr} C_{N_{LRF}}\right) T_{E_{LRF}} \tag{25.2}$$

$(\Delta E_m, \Delta N_m)$ = Instrument misalignments from Eqs. (13.2), (23.2) and (23.3)

$$\begin{aligned}\Delta E_m &= \Delta E_{mf} + \Delta E_{mo} \\ &= -m_{f1}\, C_N - m_{f2} S_N - (m_{f3} - m_{\eta 1} - m_{\eta 3})B + 2m_{\eta 2} - \Delta E_{moe}\end{aligned} \tag{26.1}$$

$$\begin{aligned}\Delta N_m C_E &= (\Delta N_{mf} + \Delta N_{mo})C_E = -m_{f2}\, C_N + m_{f1} S_N \\ &\quad + (m_{f3} - m_{\eta 1} - m_{\eta 3})A + (m_{Y0} + m_{Y1}\, S_E + m_{Y2}\, C_E) - \Delta N_{moe}\end{aligned} \tag{26.2}$$

Substituting Eqs. (25.1) to (26.2) in Eq. (24) leads to the combined attitude correction and misalignment equations:

$$\begin{aligned}E_{ACF} &= E_{LRF} - (\theta_{corr} C_{N_{LRF}} + \psi_{corr} S_{N_{LRF}}) + m_{f1} C_N + m_{f2} S_N \\ &\quad + (m_{f3} - m_{\eta 1} - m_{\eta 3})B - 2m_{\eta 2} + \Delta E_{moe}\end{aligned} \tag{27.1}$$

$$\begin{aligned}N_{ACF} &= N_{LRF} - \phi_{corr} - \left(\theta_{corr} S_{N_{LRF}} - \psi_{corr} C_{N_{LRF}}\right) T_{E_{LRF}} + m_{f2}\, C_N / C_E - m_{f1} S_N / C_E \\ &\quad - (m_{f3} - m_{\eta 1} - m_{\eta 3})A - (m_{Y0}/C_E + m_{Y1}\, T_E + m_{Y2}) + \Delta N_{moe}\end{aligned} \tag{27.2}$$

Rearranging terms in Eqs. (27.1) and (27.2) using Eqs. (22.2), (22.3), (23.4) and (23.5) with $(E_{LRF}, N_{LRF}) \cong (E, N) + (A, B)$, $C_{x+\Delta x} \cong C_x - \Delta x\, S_x$, and $S_{x+\Delta x} \cong S_x + \Delta x$ lead to:

$$\begin{aligned}&C_{N_{LRF}} \cong C_N - BS_N,\ C_{E_{LRF}} \cong C_E - AS_E,\ S_{N_{LRF}} \cong S_N + B,\ S_{E_{LRF}} \cong S_E + A, \\ &S_{N_{LRF}} T_{E_{LRF}} \cong S_N T_E + BS_E + AS_N,\ T_{N_{LRF}} T_{E_{LRF}} \cong S_N S_E + BS_E + AS_N\end{aligned} \tag{27.3}$$

$$\begin{aligned}E_{ACF} &= E_{LRF} - [(\theta_{corr} - m_{f1} + 2m_{\eta 2}) C_{N_{LRF}} + \psi_{corr} S_{N_{LRF}}] + m_{f2} S_N \\ &\quad + (m_{f3} - m_{\eta 1} - m_{\eta 3})B - 2m_{\eta 2}(1 - C_N) + \Delta E_{moe} + \Delta E_{mfe}\end{aligned} \tag{27.4}$$

$$\begin{aligned}N_{ACF} &= N_{LRF} - (\phi_{corr} - m_{f2} + m_{\eta 1} + m_{\eta 3}) \\ &\quad - [\left(\theta_{corr} - m_{f1} + 2m_{\eta 2}\right) S_{N_{LRF}} - \psi_{corr} C_{N_{LRF}}\big) T_{E_{LRF}} - m_{f2}(1 - C_N/C_E) \\ &\quad - m_{f1} S_N / C_E - (m_{f3} - m_{\eta 1} - m_{\eta 3})A - m_{Y0}(1 - C_E)/C_E \\ &\quad - m_{Y1} T_E - \left(m_{f1} - 2m_{\eta 2}\right) S_N T_E + \Delta N_{moe} + \Delta N_{mfe}\end{aligned} \tag{27.5}$$

Where,

$$\Delta E_{moe} = -m_{Y1} BS_E\ ,\ \Delta N_{moe} = m_{Y1} AS_E - 2m_{\eta 2} BS_E \tag{28.1}$$
$$\Delta E_{mfe} = -(m_{f1} - 2m_{\eta 2})(C_{N_{LRF}} - C_N) = (m_{f1} - 2m_{\eta 2}) BS_N \tag{28.2}$$
$$\Delta N_{mfe} = -\left(m_{f1} - 2m_{\eta 2}\right)\left(S_{N_{LRF}} T_{E_{LRF}} - S_N T_E\right) = -\left(m_{f1} - 2m_{\eta 2}\right)(BS_E + AS_N) \tag{28.3}$$

Redefining the attitude correction angles and the misalignment parameters in Eq. (24) to match Eqs. (27.4) and (27.5), we get

$$E_{ACF} = E_{LRF} - \Delta E'_{corr} - \Delta E'_m \text{ , } N_{ACF} = N_{LRF} - \Delta N'_{corr} - \Delta N'_m \tag{29.1}$$

$$\Delta E'_{corr} = (\theta_{corr} - m_{f1} + 2m_{\eta 2})C_{N_{LRF}} + \psi_{corr}S_{N_{LRF}} = \left(\theta'_{corr}C_{N_{LRF}} + \psi'_{corr}S_{N_{LRF}}\right) \tag{29.2}$$

$$\begin{aligned}\Delta N'_{corr} &= \left(\phi_{corr} - m_{f2} + m_{\eta 1} + m_{\eta 3}\right) \\ &\quad +[(\theta_{corr} - m_{f1} + 2m_{\eta 2})S_{N_{LRF}} - \psi_{corr}C_{N_{LRF}}]T_{E_{LRF}} && (29.3) \\ &= \phi'_{corr} + \left(\theta'_{corr}S_{N_{LRF}} - \psi'_{corr}C_{N_{LRF}}\right)T_{E_{LRF}} && (29.4)\end{aligned}$$

Where,

$$\begin{bmatrix}\phi'_{corr} \\ \theta'_{corr} \\ \psi'_{corr}\end{bmatrix} = \begin{bmatrix}\phi_{corr} \\ \theta_{corr} \\ \psi_{corr}\end{bmatrix} - \begin{bmatrix}m_{f2} - m_{\eta 1} - m_{\eta 3} \\ m_{f1} - 2m_{\eta 2} \\ 0\end{bmatrix} \tag{29.5}$$

Redefining the misalignment parameters in Eq. (29.1) to match Eqs. (27.4) and (27.5) and using Eqs. (21.5), (22.2), (23.4), (28.1), and (28.2) lead to:

$$\begin{aligned}\Delta E'_m &= -m_{f2}S_N + 2m_{\eta 2}(1 - C_N) - (m_{f3} - m_{\eta 1} - m_{\eta 3})B - \Delta E_{me} \\ &= -\phi_m S_N + O_{m2}(1 - C_N) + \psi_m B - \Delta E_{me} && (30.1) \\ \Delta N'_m &= m_{f2}(1 - C_N/C_E) + m_{f1}S_N/C_E + (m_{f3} - m_{\eta 1} - m_{\eta 3})A \\ &\quad + m_{Y0}\,(1 - C_E)/C_E + m_{Y1}\,T_E + \left(m_{f1} - 2m_{\eta 2}\right)S_N T_E - \Delta N_{me} \\ &= \phi_m(1 - C_N/C_E) + \theta_m S_N(1 + S_E)/C_E + O_m T_E \\ &\quad + O_{m1}(1 - C_E)/C_E - O_{m2}S_N T_E - \psi_m A - \Delta N_{me} && (30.2)\end{aligned}$$

This leads to:

$$\begin{bmatrix}\phi_m \\ \theta_m \\ O_m \\ O_{m1} \\ O_{m2} \\ \psi_m\end{bmatrix} = \begin{bmatrix}\text{Roll} \\ \text{Pitch} \\ \text{Orthogonality} \\ \text{Orthogonality1} \\ \text{Orthogonality2} \\ \text{Yaw}\end{bmatrix}_{\text{Misalignment}} = \begin{bmatrix}m_{f2} \\ m_{f1} \\ -0.5\left(m_{\eta 1} + m_{\eta 3} - m_{e1} + m_{e3}\right) \\ 0.75\left(m_{\eta 1} + m_{\eta 3} - m_{e1}\right) + 0.25\,m_{e3} \\ 2m_{\eta 2} \\ -m_{f3} + m_{\eta 1} + m_{\eta 3}\end{bmatrix} \tag{30.3}$$

$$\Delta E_{me} = \Delta E_{moe} + \Delta E_{mfe} = -O_m B S_E + (\theta_m - O_{m2})B S_N \tag{30.4}$$

$$\Delta N_{me} = \Delta N_{moe} + \Delta N_{mfe} = O_m A S_E - \theta_m B S_E - (\theta_m - O_{m2})A S_N \tag{30.5}$$

Therefore, the improved misalignment equations are given by:

$$\begin{bmatrix}E_{IIRF} \\ N_{IIRF}\end{bmatrix} = \begin{bmatrix}E_{LRF} \\ N_{LRF}\end{bmatrix} - \begin{bmatrix}\Delta E'_m \\ \Delta N'_m\end{bmatrix} = \begin{bmatrix}E_{LRF} \\ N_{LRF}\end{bmatrix} - h_m SV_m + \begin{bmatrix}\Delta E_{me} \\ \Delta N_{me}\end{bmatrix} \tag{31.1}$$

$$h_m = \begin{bmatrix}-S_N & \vdots & 0 & \vdots & 0 & \vdots & 0 & \vdots & 1 - C_N & \vdots & B \\ 1 - \frac{C_N}{C_E} & \vdots & \frac{S_N}{C_E}(1 + S_E) & \vdots & T_E & \vdots & (1 - C_E)/C_E & \vdots & -T_E S_N & \vdots & -A\end{bmatrix} \tag{31.2}$$

$$SV_m = [\phi_m \;\; \theta_m \;\; O_m \;\; O_{m1} \;\; O_{m2} \;\; \psi_m]^T \tag{31.3}$$

Note that Eqs. (29.1) to (31.3) are useful for verifying the accuracy of the misalignment model used in Kalman Filter [1] by comparing (E_{ACF}, N_{ACF}) of Eq. (29.1) with the values obtained from NASTRAN thermoelastic (also called thermal distortion) analysis. The 9 states in Eqs. (29.5) and (30.3), however, are determined by the Kalman Filter [1] without need to know their relationship to the primitive misalignment angles.

It should be mentioned that the yaw misalignment state ψ_m determination requires star and/or landmark measurements to be located at maximum separation from the FPM center. This is because the measurement residuals are not sensitive to ψ_m for measurements at the FPM center (i.e., A=B=0). If this complicates INR operation, a special on orbit test (or inspection of level 1B swath to swath imagery data) can determine ψ_m bias (i.e., constant term). The use of this bias in Eq. (31.3) would at least reduce (but not eliminate) ψ_m effect on INR performance. The special test consists of sighting a star (or a landmark) 3 times. The first time t_1 determines the location of the star (or landmark) within the FPM, second time t_2 makes the star (or landmark) located near the extreme south of the FPM, and third time t_3 makes the star (or landmark) located near the extreme north of FPM. The ψ_m bias is then computed from $\psi_m = (E_3 - E_2)/(N_3 - N_2)$, where (E_2, E_3) are the second and third star (or landmark) EW locations and (N_2, N_3) are the corresponding NS locations. Note that the third measurement must be rectified to the time of the second measurement. This rectification is performed using spacecraft attitude telemetry and orbit knowledge to subtract spacecraft attitude and orbit effects on star (or landmark) motion relative to spacecraft between t_2 to t_3.

Note also that if some of $(\Delta E_{me}, \Delta N_{me})$ modeling error terms in Eqs. (30.4) and (30.5) are determined to be significant to meet INR requirements, h_m of Eq. (31.2) can simply be redefined to include these significant terms.

5 INR Improvement for Single Mirror Instruments

The use of Eq. (31.3) instead of the classical $SV_m = [\phi_m \quad \theta_m]^T$ in GOES I-M and MTSAT-1R type instruments is expected to improve INR performance. This is described in the following two subsections.

5.1 GOES I-M Type Instruments

The yaw misalignment ψ_m has insignificant effect because the visible array dimension is 1 km x 8 km and the IR array dimension is 4 km x 8 km (see pages 28 and 29 of Ref. [4]). Therefore, using Eqs. (31.2) and (31.3) with (A, B) = (56, 112) μrad, a misalignment yaw ψ_m =1000 μrad produces (EW, NS) errors = (ΔE, ΔN) ≈ (0.112,0.056) μrad which are insignificant. On the other hand, the orthogonality O_m due to thermal variation and/or bias of 500 μrad produces large NS star measurement residual error = O_m Tan E ≈ 100 μrad (= 20% of O_m) at E = 11° and NS landmark measurement residual error = O_m Tan E ≈ 75 μrad at E = 8.7° . This error has small effect on frame-to-frame registration but has significant effect (≈150 μrad = 30% of O_m) on within frame registration. The secondary orthogonality misalignments (O_{m1}, O_{m2}) thermal variation and/or bias of 500 μrad produces smaller EW and NS errors because their effects on INR performance is multiplied by $(1-C_E)$ and $(1-C_N)$.

This suggests that Kalman Filter INR software design should be based on deleting ψ_m, $O_{m1}$and/or O_{m2} if proven to be insignificant by analysis and/or during In Orbit Test (IOT).

5.2 MTSAT-1R Type Instruments

MTSAT-1R FPM dimension is about 26 km x 336 km (see Fig. 5 of Ref. [5]). Therefore, Therefore, using Eqs. (31.2) and (31.3) with (A, B) = (364, 4704) μrad and ψ_m = 1000 μrad produces (ΔE, ΔN) ≈ (4.7, 0.4) μrad errors. The orthogonality and the secondary orthogonality angles (O_m, O_{m1}, O_{m2}) produce the same errors described in Sect. 5.1.

During MTSAT-1R IOT, large residual errors between the actual INR measurements and their predicted values led to unsatisfactory imagery products. Many hypotheses were advanced to explain these errors during rigorous, extensive testing and analysis of the daily landmark residual plots led by Mr. Seiichiro Kigawa of Japan Meteorological Agency (JMA). This analysis concluded the existence of systematic errors, but none led to effective correction. To minimize cost and schedule delays of a protracted investigation, ParSEC method was developed and later patented [6] that could remove these systematic errors without the need to know their origin. In this new method, the various residual errors are modeled in terms of a power series whose coefficients are determined by a least squares algorithm to minimize the landmark residuals. The ParSEC algorithm [6, 7] corrects the detected scan angles (E, N) from a distorted raw image into a non-distorted (E′, N′) space as

$$(E', N') = (E, N) - (\Delta E, \Delta N) \quad (32.1)$$

$$\Delta E = A_0 + A_1 E + A_2 N + A_3 EN + A_4 E^2 + A_5 N^2 \quad (32.2)$$

$$\Delta N = B_0 + B_1 E + B_2 N + B_3 EN + B_4 E^2 + B_5 N^2 \quad (32.3)$$

(E, N) = Instrument scan angles from raw image
(ΔE, ΔN) = ParSEC correction angles
(E′, N′) = ParSEC) corrected scan angles
(A_i, B_i) = (ΔE, ΔN) power series i^{th} ParSEC coefficient

The navigation solution residuals after implementation of this method [6] were typically about 14 μrad for stars (~1 raw visible star sense pixel), 20 μrad for visible landmarks (~2/3 visible image pixel), and 40 rad for IR landmarks (~1/3 IR image pixels), which were consistent with expected INR performance.

Note that some of the terms in Eqs. (32.2) and (32.3) are covered by the improved misalignment Eqs. (31.1) to (31.3) (using cos x ≅ 1- x^2/2, sin x ≅ x) and were not covered by the first two columns of Eq. (31.2) that was available at MTSAT-1R time. Most likely, these were the unknown source of the systematic errors. In this case, the improved misalignment Eqs. (31.1) to (31.3) could eliminate future need for the ParSEC algorithm [10].

6 Two Mirror Instruments Nominal Optical Path

The simplified Fig. 7 shows the relation of the reflected $\hat{R}_e$ and $\hat{R}_n$ optical path to the incident $\hat{I}$ optical path that emanates from the center C_I of the FPM Image (FPM_I) at the telescope port near the EW scan mirror.

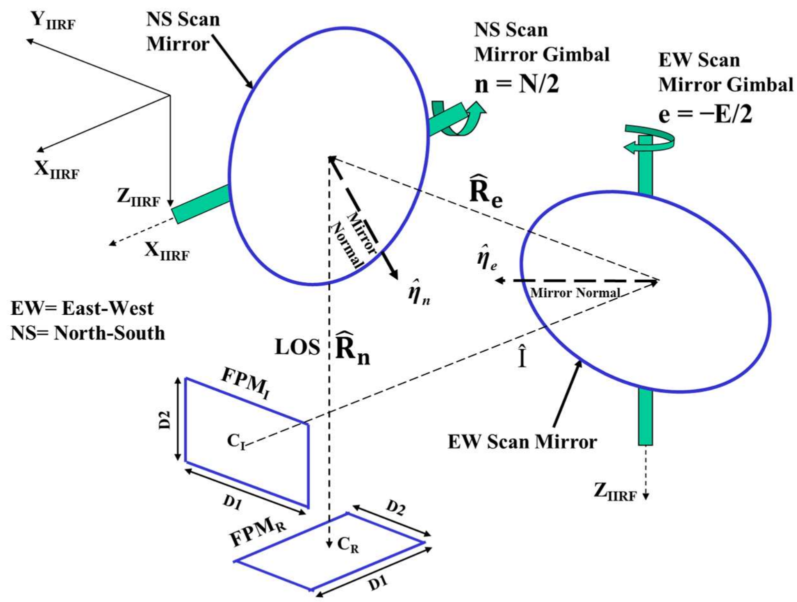

Fig. 7 Relation of Reflected Optical Path to Incident Optical Path

6.1 Instrument Gimbal Angles

In Fig. 7, (e, n) are rotations about (Z_{IIRF}, X_{IIRF}) axes, the incident unit vector $\hat{I}$ is nominally along the $-X_{IIRF}$ axis, and the FPM_I is nominally in the (Y_{IIRF}, Z_{IIRF}) plane. In this case, when the scan mirrors are at their home (or nadir) position (i.e., e = n = 0), the reflected unit vector $\hat{R}_e$ is along the Y_{IIRF}. The reflected unit vector $\hat{R}_n$ represents the instrument LOS and is along the Z_{IIRF} axis. The reflected FPM_R is in the (X_{IIRF}, Y_{IIRF}) plane. The unit vector $\hat{\eta}_e$ is normal to the EW mirror and is in the (X_{IIRF}, Y_{IIRF}) plane. The unit vector $\hat{\eta}_n$ is normal to the NS mirror and is in the (Y_{IIRF}, Z_{IIRF}) plane. The angle e is the mechanical EW shaft rotation angle about the Z_{IIRF} axis such that positive e moves LOS to the west. The angle n is the mechanical NS shaft rotation angle about the X_{IIRF} axis such that positive n moves LOS to the north.

The relation of the EW optical angle E to the mechanical EW shaft angle e is $E = -2e$ based on Snell's law, where E is positive East. Similarly, the relation of the NS optical angle

N to the mechanical shaft angle n is N = 2 n, where N is positive north. Also, the reflected EW and NS vectors are given by the Householder transformation:

$$\hat{R}_e = \hat{I} - 2(\hat{\eta}_e \bullet \hat{I})\hat{\eta}_e, \hat{R}_n = \hat{R}_e - 2(\hat{\eta}_n \bullet \hat{R}_e)\hat{\eta}_n \tag{33}$$

To compute the ray vector from the FPM_I to FPM_R in Fig. 7, the normal to the scan mirror surface must be known. The mirror normal $\hat{\eta}_0$ (renamed $\hat{\eta}_{e0}$) has equal X_{IIRF} and Y_{IIRF} components and a zero Z_{IIRF} component. This leads to:

$$\hat{I} = -\begin{bmatrix}1\\0\\0\end{bmatrix},\ \hat{\eta}_{e0} = \frac{1}{\sqrt{2}}\begin{bmatrix}1\\1\\0\end{bmatrix}, \hat{\eta}_e = \begin{bmatrix}C_e & -S_e & 0\\ S_e & C_e & 0\\ 0 & 0 & 1\end{bmatrix}\hat{\eta}_{e0} = \frac{1}{\sqrt{2}}\begin{bmatrix}Y_e\\X_e\\0\end{bmatrix} \tag{34.1}$$

$$X_e = C_e + S_e = (1 - S_E)^{1/2}, Y_e = C_e - S_e = (1 + S_E)^{1/2} \tag{34.2}$$

$$\hat{R}_e = \begin{bmatrix}(Y_e^2 - 1) & X_eY_e & 0\end{bmatrix}^T = \begin{bmatrix}S_E & C_E & 0\end{bmatrix}^T \tag{34.3}$$

Similarly, the mirror normal $\hat{\eta}_{n0}$ has equal $-Y_{IIRF}$ and Z_{IIRF} components and a zero X_{IIRF} component. This leads to:

$$\hat{\eta}_{n0} = \frac{1}{\sqrt{2}}\begin{bmatrix}0\\-1\\1\end{bmatrix}, \hat{\eta}_n = \begin{bmatrix}1 & 0 & 0\\ 0 & C_n & -S_n\\ 0 & S_n & C_n\end{bmatrix}\hat{\eta}_{n0} = \frac{1}{\sqrt{2}}\begin{bmatrix}0\\-Y_n\\X_n\end{bmatrix} \tag{35.1}$$

$$X_n = C_n - S_n = (1 - S_N)^{1/2}, Y_n = C_n + S_n = (1 + S_N)^{1/2} \tag{35.2}$$

$$\hat{R}_n = \begin{bmatrix}S_E & -C_E(Y_n^2 - 1) & C_EX_nY_n\end{bmatrix}^T = \begin{bmatrix}S_E & -S_NC_E & C_NC_E\end{bmatrix}^T \tag{35.3}$$

Eq. (35.3) is the same as Eq. (5.2) for single mirror and can be visualized in Fig. 2.

6.2 *Off-Center Detector Image Reflection*

The off-center detector image reflection can be determined using Eqs. (33) to (35.3) with the incident unit vector $\hat{I}$ in Fig. 7 changed to represent a point off the center C_I of the FPM_I image. The left side of Fig. 8 shows the case when the point P_I is at (Y_{IIRF}, Z_{IIRF}) = (a, b). In this case, the (Y_{IIRF}, Z_{IIRF}) components of the incident unit vector $\hat{I}$ are $(-\ a, -\ b)$ and is rewritten as:

$$\hat{I} = [-c\ \vdots -b\ \vdots -a]^T, c = \sqrt{1 - a^2 - b^2} \tag{36}$$

Now substituting $\hat{I}$ of Eq. (36), $\hat{\eta}_e$ of Eq. (34.1), and $\hat{\eta}_n$ of Eq. (35.1) in Eq. (33), we get:

$$\hat{R}_n = \begin{bmatrix}\hat{R}_{nX}\\ \hat{R}_{nY}\\ \hat{R}_{nZ}\end{bmatrix} = c\begin{bmatrix}S_E\\ -S_NC_E\\ C_NC_E\end{bmatrix} + \begin{bmatrix}aC_E\\ aS_NS_E - bC_N\\ -aC_NS_E - bS_N\end{bmatrix} = \begin{bmatrix}S_{E_{LRF}}\\ -S_{N_{LRF}}C_{E_{LRF}}\\ C_{N_{LRF}}C_{E_{LRF}}\end{bmatrix} \tag{37}$$

This leads to:

$$\begin{bmatrix}E_{LRF}\\ N_{LRF}\end{bmatrix} = \begin{bmatrix}\mathrm{Sin}^{-1}(cS_E + aC_E)\\ \mathrm{Tan}^{-1}(\frac{cS_NC_E - aS_NS_E + bC_N}{cC_NC_E - aC_NS_E - bS_N})\end{bmatrix} \equiv \begin{bmatrix}E_{IIRF}\\ N_{IIRF}\end{bmatrix} \text{ with no misalignments} \tag{38.1}$$

$$(X_{LRF}, Y_{LRF}, Z_{LRF}) \equiv (X_{IIRF}, Y_{IIRF}, Z_{IIRF}) \text{ with no misalignments} \tag{38.2}$$

In view of Eq. (37) and Fig. 8, the FPM center (0,0) is reflected at the point (S_E, $-S_N C_E$) in the FOR. Also, the point P_R deviation (ΔR_{nx}, ΔR_{ny}) from the reflected FPM center can be obtained from Equation (37) as follows:

$$\begin{bmatrix}\Delta\hat{R}_{nX}\\ \Delta\hat{R}_{nY}\end{bmatrix} = \begin{bmatrix}S_{E_{LRF}}\\ -S_{N_{LRF}}C_{E_{LRF}}\end{bmatrix} - \begin{bmatrix}S_E\\ -S_N C_E\end{bmatrix} = (c-1)\begin{bmatrix}S_E\\ -S_N C_E\end{bmatrix} + \begin{bmatrix}aC_E\\ aS_N S_E - bC_N\end{bmatrix} \qquad (39)$$

Where, (E_{LRF}, N_{LRF}) are the detector LOS EW and NS angles to the point P_R and (E, N) are the Instrument LOS EW and NS scan angles [i.e., = 2(−e, n), where (e, n) are the EW and NS shaft angles].

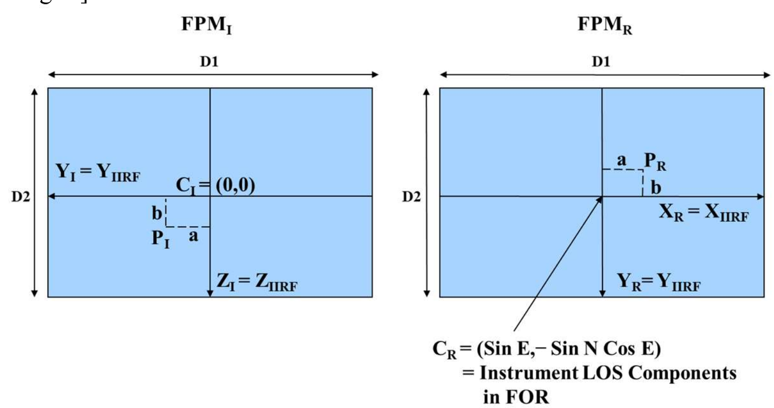

Fig. 8 Two-Mirror Design Avoids Detector Rotation About FPM Center

Now, the deviation in the P_R pointing angles (E_{LRF}, N_{LRF}) from the FPM LOS pointing angle (E, N) can be obtained by substituting $(E_{LRF}, N_{LRF}) = (E, N) + (\Delta E, \Delta N)$ in Eq. (39). Ignoring the higher order terms in (ΔE, ΔN), we get:

$$\begin{bmatrix}\Delta\hat{R}_X\\ \Delta\hat{R}_Y\end{bmatrix} = \begin{bmatrix}\Delta E\ C_E\\ -\Delta N C_N C_E + \Delta E S_N S_E\end{bmatrix} = \begin{bmatrix}aC_E\\ aS_N S_E - bC_N\end{bmatrix} \qquad (40.1)$$

$$(\Delta E, \Delta N) \cong (a, b/C_E) \text{ and } (E_{LRF}, N_{LRF}) \cong (E, N) + (a, b/C_E) \qquad (40.2)$$

Note that the b component is divided by C_E to convert it to ΔN like Eq. (9.2) for single mirror. Note also that, in view of Fig. 8 and Eq. (40.2), the two mirrors eliminate the FPM image rotation shown in Fig. 5 and Eq. (9.2). Therefore, future hardware improvements can lead to meeting INR requirements without need for ground resampling. This can be achieved by instrument yaw misalignment (ψ_m) minimized prior to launch, instrument operation with on-board autonomous image navigation, accurate Image Motion Compensation (IMC) computation [1], sample and hold of pixel data, and spacecraft operation with x-axis parallel to earth equator and yaw attitude minimized by the control system. Note also that the instrument and spacecraft yaw angles are further attenuated by (b, a) to get its effect on INR (EW, NS) errors when the IMC is on.

7 Two Mirror Optical Path with Misalignments

The misalignments in Fig. 7 can be summarized as it was done in section 3 as follows:

- FPM center and axes misalignments relative to the EW scan mirror represented by small offsets (m_{f1}, m_{f2}) along the (Y_{IIRF}, Z_{IIRF}) axes and a small rotation m_{f3} about the X_{IIRF} axis.
- EW scan mirror normal orthogonality misalignment relative to the IIRF frame represented by small rotations ($m_{\eta e1}$, $m_{\eta e2}$, $m_{\eta e3}$) about the (X_{IIRF}, Y_{IIRF}, Z_{IIRF}) axes. The mirror rotation axis orthogonality misalignment relative to the IIRF frame represented by small rotations (m_{e1}, m_{e2}, m_{e3}) about the (X_{IIRF}, Y_{IIRF}, Z_{IIRF}) axes.
- NS scan mirror normal orthogonality misalignment relative to the IIRF frame represented by small rotations ($m_{\eta n1}$, $m_{\eta n2}$, $m_{\eta n3}$) about the (X_{IIRF}, Y_{IIRF}, Z_{IIRF}) axes. The mirror rotation axis orthogonality misalignment relative to the IIRF frame represented by small rotations (m_{n1}, m_{n2}, m_{n3}) about the (X_{IIRF}, Y_{IIRF}, Z_{IIRF}) axes.

Now, following similar approach as in Sects. 3 and 4 leads to:

$$E_{ACF} = E_{LRF} - \Delta E'_{corr} - \Delta E'_m \ , \ N_{ACF} = N_{LRF} - \Delta N'_{corr} - \Delta N'_m \tag{41}$$

$$\Delta E'_{corr} = \theta'_{corr} C_{N_{LRF}} + \psi'_{corr} S_{N_{LRF}} \tag{42.1}$$

$$\Delta N'_{corr} = \phi'_{corr} + \left(\theta'_{corr} S_{N_{LRF}} - \psi'_{corr} C_{N_{LRF}}\right) T_{E_{LRF}} \tag{42.2}$$

$$\begin{bmatrix} \phi'_{corr} \\ \theta'_{corr} \\ \psi'_{corr} \end{bmatrix} = \begin{bmatrix} \phi_{corr} \\ \theta_{corr} \\ \psi_{corr} \end{bmatrix} - \begin{bmatrix} m_{f2} - m_{\eta e1} + m_{\eta e2} + 2m_{\eta n1} \\ m_{f1} + m_{\eta n2} + m_{\eta n3} - 2m_{\eta e3} \\ \frac{1}{2}\left(m_{\eta n3} + m_{\eta n2} + m_{n3} - m_{n2}\right) \end{bmatrix} \tag{42.3}$$

$$\Delta E'_m = O_{m2}(1 - C_N) + \psi_m b - \Delta E_{me} \tag{43.1}$$

$$\Delta N'_m = O_m T_E + O_{m1}(1 - C_E)/\,C_E - O_{m2} T_E S_N - \psi_m a - \Delta N_{me} \tag{43.2}$$

$$\begin{bmatrix} O_m \\ O_{m1} \\ O_{m2} \\ \psi_m \end{bmatrix} = - \begin{bmatrix} -\frac{1}{2}(m_{\eta e1} - m_{\eta e2} - m_{e2} - m_{e1} + m_{\eta n2} + m_{\eta n3} + m_{n2} - m_{n3}) \\ m_{f2} + \frac{1}{4} m_{e2} - \frac{3}{4}(m_{\eta e1} - m_{\eta e2} - m_{e1}) \\ m_{f1} - 2m_{\eta e3} + \frac{3}{4}(m_{\eta n2} + m_{\eta n3} - m_{n2}) + \frac{1}{4} m_{n3} \\ m_{f3} + m_{\eta e1} - m_{\eta e2} + \frac{1}{2}(m_{\eta n2} + m_{\eta n3} + m_{n2} - m_{n3}) \end{bmatrix} \tag{43.3}$$

Where (O_m , O_{m1}, O_{m2}, ψ_m) = (Orthogonality, Orthogonality1, Orthogonality2, Yaw) misalignments were introduced by Kamel during his INR support (2005-2008) of GOES-R Advanced Baseline Imager (ABI) implementation phase at ITT. This leads to:

$$\begin{bmatrix} E_{IIRF} \\ N_{IIRF} \end{bmatrix} = \begin{bmatrix} E_{LRF} \\ N_{LRF} \end{bmatrix} - \begin{bmatrix} \Delta E'_m \\ \Delta N'_m \end{bmatrix} = \begin{bmatrix} E_{LRF} \\ N_{LRF} \end{bmatrix} - h_m SV_m + \begin{bmatrix} \Delta E_{me} \\ \Delta N_{me} \end{bmatrix} \tag{44.1}$$

$$h_m = \begin{bmatrix} 0 & \vdots & 0 & \vdots & 1 - C_N & \vdots & b \\ T_E & \vdots & (1 - C_E)/C_E & \vdots & -T_E S_N & \vdots & -a \end{bmatrix}, \ SV_m = [O_m \ \ O_{m1} \ \ O_{m2} \ \ \psi_m]^T \tag{44.2}$$

The misalignment (ΔE_{me}, ΔE_{me}) modeling errors are given by:

$\Delta E_{me} \cong M_{E1}aS_E + M_{E2}bS_E + M_{E4}bS_N$ (45.1)

$\Delta N_{me} \cong M_{N0}S_ES_N(1\text{-}0.5S_N) + M_{N1}aS_E + M_{N2}aS_N + M_{N3}bS_E + M_{N4}bS_N$ (45.2)

Where,

$M_{E1} = 2m_{\eta e3} - (m_{\eta n2} + m_{\eta n3}),\ M_{E2} = 0.5(m_{\eta e1} - m_{\eta e2} - m_{e1} - m_{e2})$ (45.3)

$M_{E4} = m_{f1} - 2m_{\eta e3} + 0.5(m_{\eta n2} + m_{\eta n3} - m_{n2} + m_{n3})$ (45.4)

$M_{N0} = 0.25(m_{\eta n2} + m_{\eta n3} - m_{n2} - m_{n3}),\ M_{N1} = 0.5(m_{\eta e1} - m_{\eta e2} + m_{e1} + m_{e2}) - 2\,m_{\eta n1}$ (45.5)

$M_{N2} = 4\,m_{\eta e3} - m_{f1} + 0.5\,(m_{n2} - m_{n3}) - 1.5(m_{\eta n2} + m_{\eta n3})$ (45.6)

$M_{N3} = 2\,m_{\eta e3} - m_{f1} - (m_{\eta n2} + m_{\eta n3}),\ M_{N4} = m_{\eta e1} + m_{\eta e2} - 2m_{\eta n1}$ (45.7)

Note that Eqs. (41) to (44.2) are like Eqs. (29.1) to (31.3). Note also that the misalignment state vector SV_m dimension = 6 for single mirror instruments and = 4 for two mirror instruments. The additional two states for single mirror are caused by (m_{f1}, m_{f2}) and FPM reflected image rotation by the NS angle N as shown by Eqs. (12.1) and (12.2) and Fig. 6.

Finally, (ΔE_{me}, ΔN_{me}) of Eqs. (45.1) and (45.2) are assumed to have insignificant effect on INR performance. If prelaunch analysis shows that they are significant, M_{N0} can be added as an INR misalignment state in Eq. (44.2) to be determined by Kalman filter and the rest of the coefficients can be determined using ParSEC method [6, 7].

8 Conclusion

Misalignment equations improvement for single mirror and two mirror instruments are shown to significantly improve INR performance. For example, (image navigation, within frame registration) improvement can be as large as (0.2 O_m , 0.3 O_m), where, O_m is scan mirror axes orthogonality misalignment due to thermal variation and measurement errors.

Appendix A: General Rotation About Misaligned Axis

Figure A shows how an arbitrary vector $\vec{A}$ rotates about a misaligned axis G_e to a vector $\vec{B}$ after a rotation by an angle e. Note that the vector $\vec{A}$ rotates such that it traces a cone about the G_e axis and therefore, the vectors $\vec{A}$ and $\vec{B}$ would have the same length. Note also that point A traces a circle about the point G and, therefore, the points A, B, and G lie in a plane perpendicular to the vector G_e. In this case, the vectors $\vec{a}$ and $\vec{b}$ also have the same length and both are perpendicular to the vector G_e. In view of Fig. A, we get:

$$\widehat{G}_e \bullet \vec{b} = 0,\ \widehat{G}_e \bullet \vec{a} = 0,\ \vec{a} \bullet \vec{b} = a^2 \mathrm{Cos}\ e = b^2 \mathrm{Cos}\ e \quad \text{(A.1)}$$

$$(\widehat{G}_e \otimes \vec{a}) \bullet \vec{b} = a^2 \mathrm{Sin}\ e = b^2 \mathrm{Sin}\ e,\ \vec{b} = \{(\vec{a} \bullet \vec{b})\vec{a} + [(\widehat{G}_e \otimes \vec{a}) \bullet \vec{b}](\widehat{G}_e \otimes \vec{a})\}/b^2 \quad \text{(A.2)}$$

Where, $\widehat{G}_e$ is a unit vector along the vector $\vec{G}_e$. This leads to:

$$\vec{b} = \vec{a}\ \mathrm{Cos}\ e + (\widehat{G}_e \otimes \vec{a})\ \mathrm{Sin}\ e,\ \vec{G}_e = \widehat{G}_e(\widehat{G}_e \bullet \vec{A}),\ \vec{a} = \vec{A} - \vec{G}_e,\ \vec{b} = \vec{B} - \vec{G}_e \quad \text{(A.3)}$$

$$\vec{B} = \vec{A} \mathrm{Cos}\ e + \widehat{G}_e(\widehat{G}_e \bullet \vec{A})(1 - \mathrm{Cos}\ e) + (\widehat{G}_e \otimes \vec{A})\ \mathrm{Sin}\ e \quad \text{(A.4)}$$

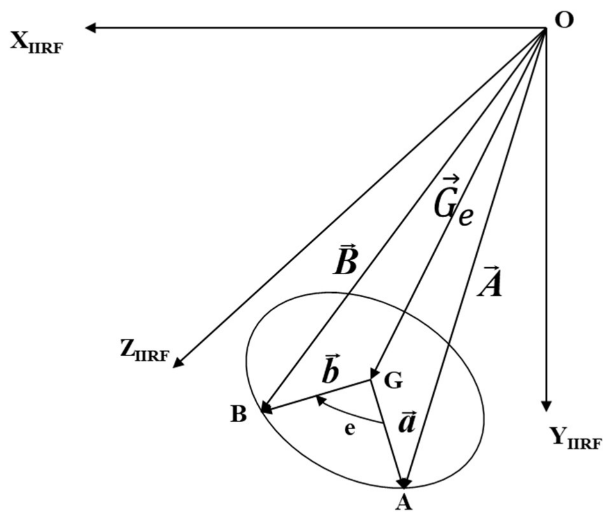

Fig. A Rotation of an Arbitrary Vector About Misaligned Gimbal Axis.

References

1. Kamel AA (2018) Generalized Image Navigation and Registration Algorithms for Ground and Space Segments, Trans. JSASS Aerospace Tech. Japan, Vol. 16 Issue 6, pp. 572-581.
2. Kamel AA, Kim H, Yang D, Park C, and Woo J (2017) Generalized Image Navigation and Registration Method Based on Kalman Filter, Advances in Aerospace Guidance, Navigation, and Control, Springer International Publishing.
3. Harris J, Kamel A, and Kim H (2009) Image Navigation and Registration Improvements using GPS, Proceedings of the 2009 IEEE International Geoscience and Remote Sensing Symposium, Vol. 3, pp. 247-250.
4. GOES I-M Data Book Prepared by Space Systems/Loral for NASA (1996) https://goes.gsfc.nasa.gov/text/goes.databook.html
5. Puschell JJ et al (2003) Japanese Advanced Meteorological Imager (JAMI) Design, Characterization and Expected On-Orbit Performance https://cimss.ssec.wisc.edu/itwg/itsc/itsc13/proceedings/posters/a28_puschell.pdf
6. Kamel AA, Sheffield J, Mclaren M (2012) Image navigation and registration accuracy improvement using parametric systematic error correction, United States Patent, 8301377. https://patentimages.storage.googleapis.com/17/1c/9e/762c11599efcd6/US8301377.pdf
7. Lyu W, Wang T, Dong Y, and Shen Y (2017) Imaging Navigation and Registration for Geostationary Imager, IEEE Geoscience and Remote Sensing letters.
8. Wertz JR (1978) Spacecraft Attitude Determination and Control, D. Reidel Publishing, Hingham (reprinted in 2000 by Kluwer Academic Publisher, Mass, Boston)
9. REDUCE http://reduce-algebra.sourceforge.net/index.php
10. Kamel AA (2019) Improved Image Navigation and Registration (INR) Algorithms, EuroGNC 2019.